Analytical and Experimental Investigation on Cutting Force in Longitudinal-Torsional Coupled Rotary Ultrasonic Machining Zirconia Ceramics

Fan Chen
Pingdingshan University
Wenbo Bie (wenbo187120@163.com)
Pingdingshan University
Yingli Chang
Pingdingshan University
Bo Zhao
Pingdingshan University
Xiaobo Wang
Pingdingshan University
Yuemin Zhang
Pingdingshan University

Research Article

Keywords: Ceramics, Cutting force, Rotary ultrasonic machining, Longitudinal-torsional coupled vibration, Analytical model

Posted Date: December 29th, 2021

DOI: https://doi.org/10.21203/rs.3.rs-1189006/v1

Version of Record: A version of this preprint was published at The International Journal of Advanced Manufacturing Technology on March 12th, 2022. See the published version at https://doi.org/10.1007/s00170-022-09031-4.

Analytical and experimental investigation on cutting force in longitudinal-torsional coupled rotary ultrasonic machining zirconia ceramics

Fan Chen[a] , Wenbo Bie[a*], Yingli Chang [a], Bo Zhao[b], Xiaobo Wang[b], Yuemin Zhang[b]

[a]Henan Province Engineering Research Center of Ultrasonic Technology Application, Pingdingshan University, Pingdingshan, China

[b]School of Mechanical and Power Engineering, Henan Polytechnic University, Jiaozuo, China

Abstract: Ceramics and other hard-and-brittle materials are very effectively processed by longitudinal-torsional coupled rotary ultrasonic machining (LTC-RUM). However, the cutting force evolution and the effects of processing parameters on the material removal mechanism in LTC-RUM need to be clarified for machining optimization. This paper proposes a cutting force model of the LTC-RUM of zirconia ceramics via the brittle material removal mechanism. Firstly, the kinematic analysis of a single abrasive grain was performed, with further consideration of the material removal volume, the effective contact time, and the impact force per one ultrasonic vibration cycle. Then, the longitudinal-torsional coupled vibration of the core tool was analyzed from the standpoint of wave energy conversion. The analytical model was finalized and experimentally verified by LTC-RUM tests. The cutting force curves predicted via the proposed model were in good agreement with the experimental results. The results obtained are considered instrumental in predicting the effects of processing parameters on cutting force during LTC-RUM of ceramics and their further optimization.

Keywords: Ceramics; Cutting force; Rotary ultrasonic machining; Longitudinal-torsional coupled vibration; Analytical model

*Corresponding author
Email address: wenbo187120@163.com

1. Introduction

Zirconia ceramics are metal oxide ceramic materials with excellent physical and chemical properties, including high mechanical strength, corrosion and wear resistance, and thermal stability. They imply their wide application in aerospace, optical, bio-medical, electronics, and other industries [1-4]. However, due to zirconia ceramics' high hardness and brittleness, obtaining their high-quality surface with conventional machining technologies is problematic, implying high tool wear and processed workpieces damage risks. In the past two decades, many innovative technologies, such as grinding [5,6], laser machining[7], electrolytic in-process dressing grinding [8], ultrasonic machining [9], ultrasonic vibration-assisted machining [10], and rotary ultrasonic machining (RUM) [11], have been introduced to mitigate the above problems.

RUM is one of the most effective ceramics-processing techniques combining material removal mechanisms of grinding and ultrasonic machining [12, 13]. Many investigations have been conducted to explore the processing characteristics of RUM, which are schematically presented in Fig.1. The research on processing advantages of RUM's hole manufacturing of brittle materials primarily can be subdivided into two main categories. The first one involves comparative studies of processing characteristics of RUM and conventional grinding, including the material removal rate [14-17], processing performance [18-20] and modeling [21-24], damage formation mechanism [25, 26], and suppression methods [27-29]. Its results proved that RUM outperforms conventional grinding by the improved the material removal rate (MRR), reduced cutting force, enhanced hole-processing accuracy and surface quality, alleviated processing damage, and extended tool life. The other research is focused on the effects of various processing factors, including tool parameters [30], the cooling condition [31], the spindle speed and feed rate [32], and ultrasonic amplitude [33], on the RUM performance. While the related studies provided more insight into the RUM perspectives for processing hard-brittle and other difficult-to-machining materials, most of them were applied to the one-dimensional (1D) RUM derived from the ultrasonic-assisted machining (UAM). Although optimizing processing parameters via 1D RUM scheme enhanced the processing performance, its capacity was restricted by the limit conditions.

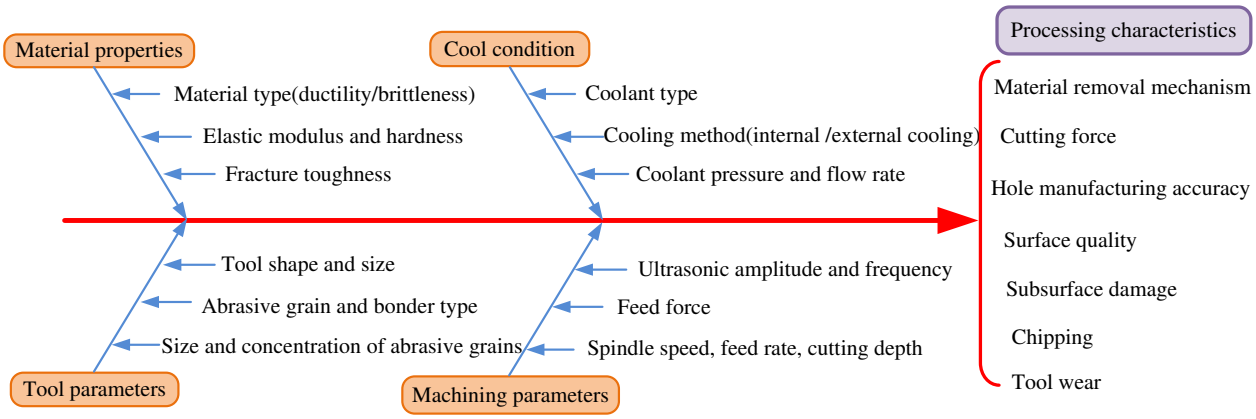

Fig. 1. Fishbone-type diagram of the major processing parameters and performance characteristics for RUM.

With the development of USM technology and the effective performance of 2D vibration in ultrasonic vibration-assisted cutting, 2D vibration has been applied to rotary ultrasonic drilling (RUD). To date, there are three types of 2D vibration, including longitudinal and bending coupled (LBC) vibration [34], double bending coupled (DBC) vibration [35], longitudinal and torsional coupled (LTC) vibration [36]. Compared with the former two types, the LTC vibration has been more widely used in different types of UAM. For instance, Gao et al.

studied the influence of longitudinal-torsional ultrasonic vibration (LTUV) on micro-hole drilling of Ti-6Al-4V. They found that the cutting force was dramatically reduced compared to conventional drilling [37]. Liu et al. developed LTUV helical milling for hole-making of carbon fiber reinforced plastic (CFRP) composites. Compared to the conventional helical milling, the LTUV-assisted one was more adapted to fracture fibers and provided better surface quality [38]. Cardoni et al. developed two types of ultrasonic drilling devices resonating in the LTUV mode, which enhanced drilling performance [39]. The above successful application of LTUV/LTC in UAM inspired the LTC-RUM application to brittle materials. Wang et al. utilized the LTC-RUM to drill ceramic matrix composites and reported that it reduced the cutting force by over 50% compared to the conventional longitudinal RUM (Con-RUM) [40]. Ma et al. experimentally investigated the processing performance of zirconia ceramics with the LTC-RUM and revealed a significant improvement of the machined surface quality compared to Con-RUM [41]. However, the material removal mechanism of LTC-RUM for brittle material has not been theoretically substantiated yet.

The cutting force is regarded as one of the most important output variables to assess the machining performance because it dramatically influences the surface damage, tool wear, cutting temperature, etc. [21]. Besides, an accurate cutting force model is required to describe the material removal mechanism during LTC-RUM. In the Con-RUM, the material removal and surface formation are related to the tool-end-face and the periphery-surface abrasive grains, which control the respective cutting forces, particularly the normal cutting force acting along the feed direction. Despite a large number of available state-of-the-art publications, to the best of the authors' knowledge, no investigations on the cutting force of LTC-RUM have been reported yet. This paper attempts to identify the material removal mechanism and simulate the cutting force in the LTC-RUM as applied to zirconia ceramics. Using the available cutting force models based on the static mechanical properties for RUM [12, 13, 21, 22], they were further refined by taking into account a single abrasive grain's kinematics analysis of LTC-RUM, tool-workpiece's intermittent interaction, effective cutting time per one ultrasonic cycle, indentation depth, and brittle fracture material removal mode. Tests were also conducted to verify the proposed mode's feasibility in predicting LTC-RUM cutting forces for various processing parameters.

2. Assumptions and approaches used in the cutting force model elaboration

2.1 Main assumptions

RUM is a complex process with many input variables: core drill diameter, concentration and size of abrasive particles, workpiece material's properties, ultrasonic parameters (ultrasonic frequency and amplitude), and machining parameters (spindle speed and feed rate). The following five assumptions were used to facilitate the LTC vibration analysis in the RUM processing of zirconia ceramics.

(1) The diamond abrasive particles were uniformly distributed along the end face of the core drill.

(2) All abrasive particles had the same size and were octahedron-shaped.

(3) The abrasive particles were perfectly rigid, had the same height and all of them participated in the cutting process in each vibration cycle.

(4) The ultrasonic frequency, amplitude, and torsional-to-longitudinal vibration ratio (A_T/A_L) remained unchanged during processing;

(5) The material removal was mainly occurred in the brittle fracture mode.

Some additional assumptions and simplifications were used, which will be provided in the following section.

2.2 The approach and main procedures used in model elaboration

The main approach and procedures used in the model's elaboration are schematically presented in Fig.2. The model development started from a single abrasive grain, its trajectory analysis, the maximum impact force, and the effective cutting time in per one vibration cycle. Based on the brittle fracture mode of the material removal, the material removal volume of a single abrasive grain was calculated by considering the abrasive grain length scratching the processed workpiece and the relevant properties of zirconia ceramics. Next, the material removal rate was assessed by superimposing all the effective abrasive grains' effects, and the cutting force evolution during LTC-RUM was predicted. Then, the actual material removal volume of a single abrasive (K_v) was adjusted for the model realization based on the additional test results. Finally, drilling tests were conducted to verify the model's feasibility and accuracy.

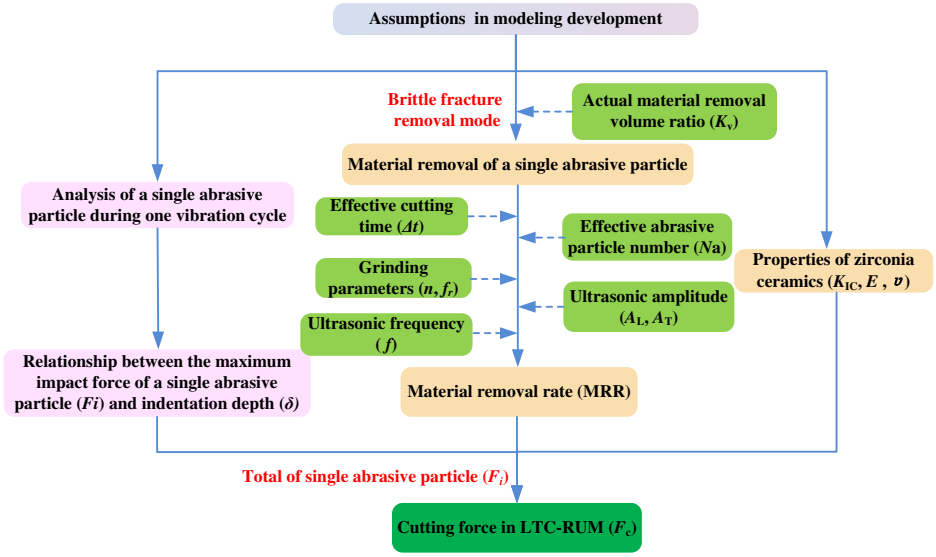

Fig. 2. The flowchart of model elaboration procedures.

3. The LTC-RUM cutting force assessment

3.1 Kinematics analysis of a single abrasive particle

In LTC-RUM processing, an electroplated diamond core drill rotated with a spindle speed n and moved toward the workpiece at a feed rate f_r, simultaneously vibrating with longitudinal amplitude of A_L and torsional amplitude A_T. The LTC-RUM scheme is depicted in Fig.3.

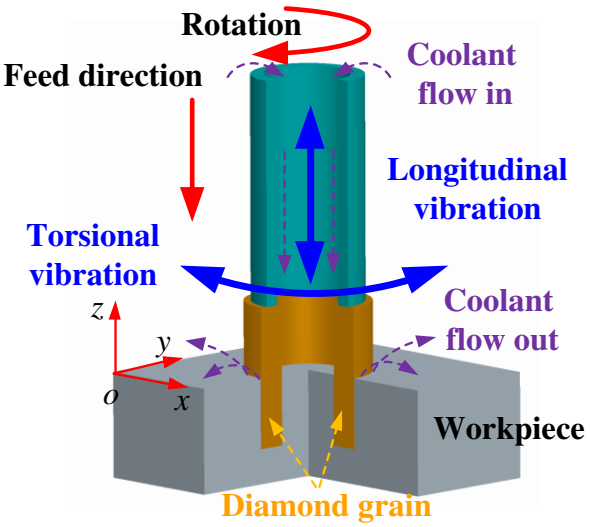

Fig.3. The LTC-RUM scheme.

During the LTC-RUM processing, the abrasive particle's axial and circumferential vibrations keep the same frequency and phase. The torsional amplitude can be approximately regarded as the arc length of rotation angle caused by torsional vibration. Therefore, the kinematic trajectory of a single abrasive particle in LTC-RUM can be expressed as follows:

$$\begin{cases} x=r\cos\left(\dfrac{A_{\mathrm{T}}}{r}\sin(2\pi ft)+\dfrac{\pi nt}{30}\right) \\ y=r\sin\left(\dfrac{A_{\mathrm{T}}}{r}\sin(2\pi ft)+\dfrac{\pi nt}{30}\right) \\ z=A_{\mathrm{L}}\sin(2\pi ft)+f_r t \end{cases} \tag{1}$$

where r is the tool's average radius. If the value of A_{T} is equal to 0, Eq.(1) can be utilized to describe the moving trajectory of an abrasive grain during Con-RUM. A diamond abrasive grain trajectory in the above two cases is illustrated in Fig.4.

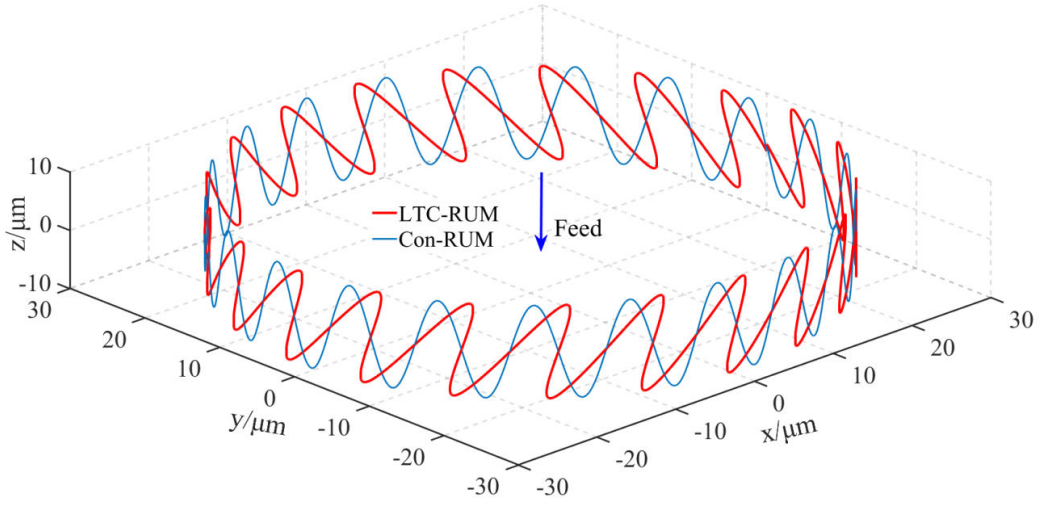

Fig.4. The motion trajectory of diamond abrasive particles in Con-RUM and LTC-RUM.

As shown in Fig.4, the abrasive particle movement trajectory in LTC-RUM is a slanted sinusoidal curve, while it is a sinusoidal curve in Con-RUM. During the LTC-RUM processing, the movement direction of abrasive particle keeps the same or opposite to the main movement direction, which leads to the intermittent cutting effect between the abrasive particle and workpiece. In order to appear the trajectory more legible in both cases, Eq.(1) can be expressed based on the cylindrical surface as follows:

$$\begin{cases} l=A_{\Gamma}\sin(2\pi ft)+2\pi rnt \\ z=A_{\mathrm{L}}\sin(2\pi ft)+f_r t \end{cases} \tag{2}$$

The grain's trajectories in the LTC-RUM and Con-RUM processing were plotted in Figs.5 and 6, respectively. Figure 5 presents the effect of ultrasonic parameters (ultrasonic frequency and amplitude) on the abrasive particle trajectory. As shown in Fig.6 (a), the abrasive grain's trajectory under the both cases was reduced with an increase in frequency. The intermittent cutting effect during LTC-RUM can be enhanced, which is beneficial to reduce the cutting force. In addition, as shown if Fig.6 (b), the ultrasonic vibration's impact effect was strengthened with an increase in the ultrasonic amplitude, increasing the grinding depth of a single abrasive grain. This promoted the material removal rate (MRR).

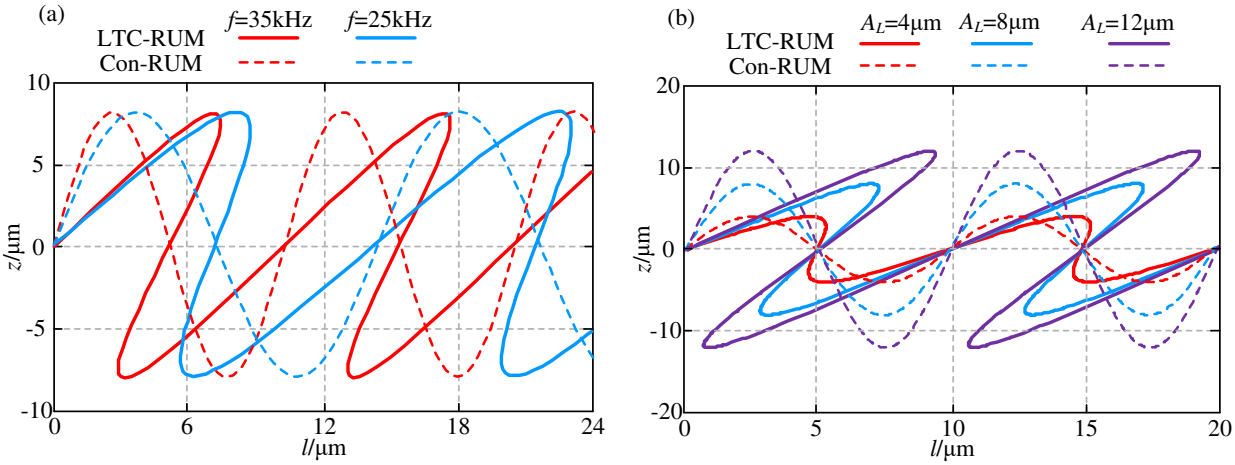

Fig.5. Effect of ultrasonic parameters on the abrasive particle trajectory. (a) Ultrasonic frequency (b) Ultrasonic amplitude.

Figure 6 presents the effect of processing parameters (spindle speed and feedrate) on the abrasive particle trajectory. With an increase in the spindle speed, as shown in Fig.6 (a), the cycloidal trajectory in a vibration cycle during both cases became sparser, i.e., the rotary pattern of abrasive grains gradually weakened, indicating that the ultrasonic vibration superiority was suppressed to a certain extent. This reduced the number of reciprocating impact ironings at the same position of the workpiece surface by different abrasive particles, and deteriorated the machined surface quality. However, the rotary pattern of abrasive grains was not obviously changed with the feed rate variation as other conditions remain constant, as shown in Fig.6 (b). This can be attributed to the fact that the feed rate was much lower than the velocity of the longitudinal ultrasonic vibration, i.e., $f_{\mathrm{r}}<<2\pi fA_{\mathrm{L}}$. Therefore, in

LTC-RUM, a suitable ultrasonic parameter should be selected to match the spindle speed in order to enhance processing efficiency and quality.

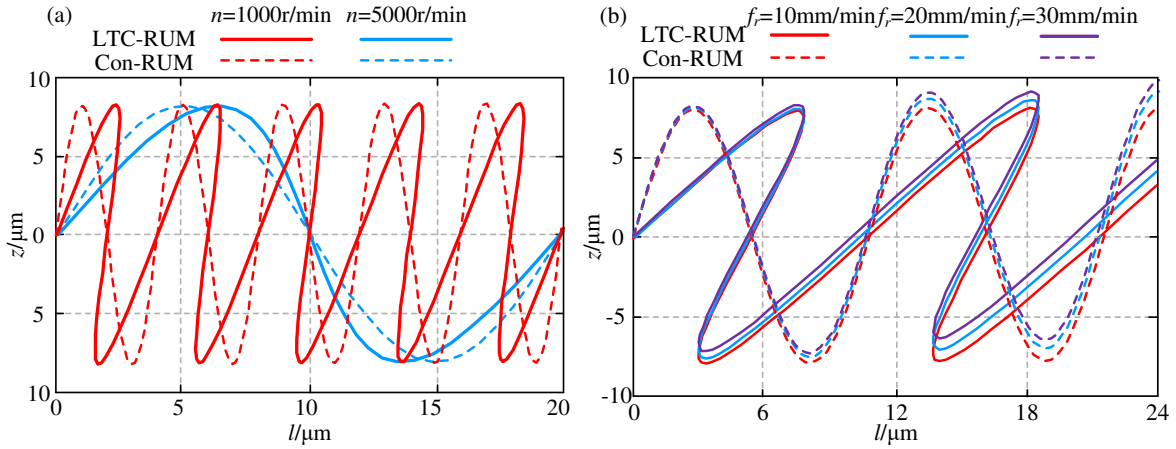

Fig.6. Effects of processing parameters on the abrasive particle trajectory. (a) spindle speed (b) feed rate.

3.2. Material removal mechanisms of ceramics

As shown in Fig.3, the trajectory of abrasive particle on the tool-end-face in LTC-RUM was not a simple superposition of Con-RUM and conventional grinding, while the abrasive grains contacted and separated with the workpiece material at an ultrasonic frequency during LTC-RUM. As depicted in Fig.7, the abrasive grain can be regarded as multiple Vickers indenters and the material firstly generated elastic and plastic deformations when the abrasive particle penetrated the workpiece. The median cracks were generated as the penetration depth continued to increase. The tensile residual stresses were generated when the abrasive particles were pulled out from the processed material, causing the lateral cracking. The cracks initiated and propagated at the workpiece's surface, promoting the material removal. Because the impact force of abrasive particle under the ultrasonic vibration on the workpiece exceeded that in conventional grinding, the material removal occurred via brittle fracture mode.

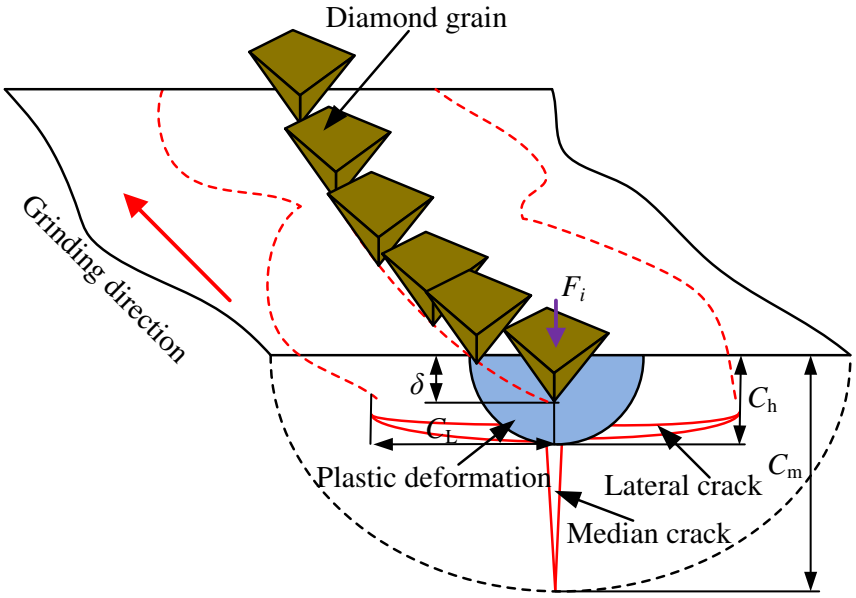

Fig. 7. The material removal mechanism related to plastic deformation and cracking.

In the LTC-RUM, the abrasive grain-workpiece contact is depicted in Fig.8, the effective contact time t_c can be calculated as.

$$t_c = \frac{\lambda}{\pi f}\left[\frac{\pi}{2} - \arcsin(1 - \frac{\delta}{A_L})\right] \tag{3}$$

where λ is a proportionality coefficient, $\lambda \in (0.5,1)$[42], δ is the indentation depth of diamond abrasive particles in the workpiece material induced by LTC-RUM.

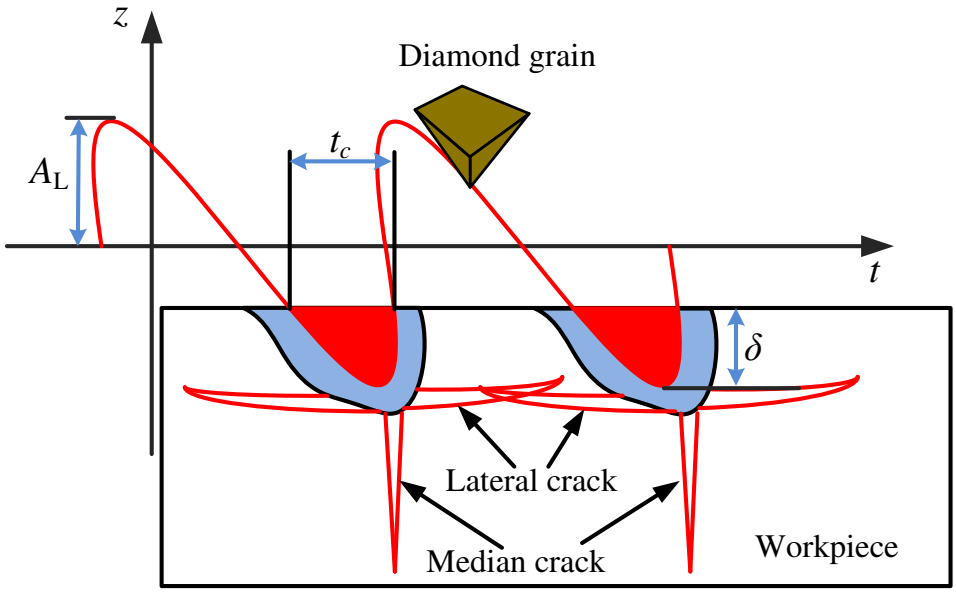

Fig.8. The abrasive grain-workpiece contact evolution.

According to the results of Liu et al. [12], the relationship between the maximum impact force of a single diamond abrasive F_i and the penetration depth δ can be expressed as:

$$F_i = 2\delta^2 H_V \tan\psi \sqrt{\tan^2\psi + 2} \tag{4}$$

where ψ=45° is the abrasive grain tip semi-angle , and H_V is the micro-hardness of the workpiece.

It is assumed that all the effective abrasive grains involved in the material removal with the same penetration depth δ, and the maximum impact force F_m of all abrasive grains can be derived as

$$F_m = N_a F_i \tag{5}$$

where N_a is the number of effective abrasive grains on the tool-end-face, which is assessed as follows:

$$N_a = \frac{\pi C_1 C_a^{2/3}}{4}\frac{\left(d_o^2 - d_i^2\right)}{S_a^2} \tag{6}$$

where C_a is the concentration of abrasive grains; Sa is the abrasive grain size; C_1 is a dimensionless constant(C_1=0.02). d_o and d_i are the outer and inner diameters of the core drill, respectively.

Since the ultrasonic frequency usually exceeds than the dynamometer's natural frequency and the processing system's resonant frequency, only the average grinding force could be measured accurately. Therefore, during the

LTC-RUM test, the measured cutting force F_c did not properly reflect the maximum impact force F_m under the action of ultrasonic vibration. Instead, based on the energy conservation theorem, the pulse (I) of the maximum impact force (F_m) during per vibration cycle can be expressed as,

$$I = \int_{cycle} F_m dt \approx F_m t_c \tag{7}$$

The pulse value I for the cutting force F_c during per vibration cycle can be written as

$$I = \frac{F_c}{f} \tag{8}$$

The relationship between F_c and F_m can be obtained by equating pulses in Eqs. (7) and (8).

$$F_c = F_m f t_c \tag{9}$$

By substituting Eqs.(3)-(6) into Eq.(9), it could be obtained:

$$F_i = \frac{\pi}{\lambda N_a}\left[\frac{\pi}{2} - \arcsin(1 - \frac{\delta}{A_L})\right]^{-1} F_c \tag{10}$$

Substituting Eq.(10) in to Eq.(4), the penetration depth δ can be calculated by the following equation.

$$\delta = \left(\frac{F_c}{2\lambda N_a H_V \tan\psi\sqrt{\tan^2\psi + 2}[(1/2) - (1/\pi)\arcsin(1 - \delta / A_L)]}\right)^{1/2} \tag{11}$$

During the LTC-RUM processing of brittle materials, material removal leadingly occurs by the brittle fracture mode. As shown in Fig.9, the single diamond grain impact on the workpiece generated the lateral and medial cracks. The material was removed by propagation and coalescence of lateral cracks.

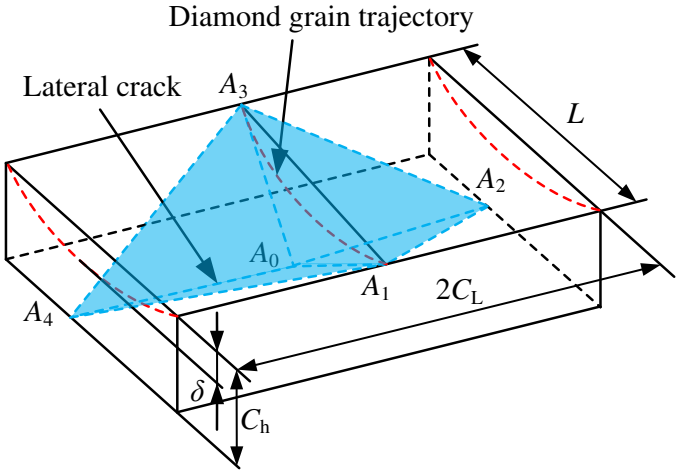

Fig.9. Calculation of material removal volume of the fracture zone

According to Wang et al. [29], the lateral crack's length (C_L) and depth (C_h) can be calculated as:

$$\begin{cases} C_L = C_2\left(\dfrac{1}{\tan\psi}\right)^{5/12}\left(\dfrac{E^{3/4}}{H_V K_{IC}(1-\upsilon^2)^{1/2}}\right)^{1/2}(F_i)^{5/8} \\ C_h = C_2\left(\dfrac{1}{\tan\psi}\right)^{1/3}\dfrac{E^{1/2}}{H_V}(F_i)^{1/2} \end{cases} \tag{12}$$

where, υ, $K_{IC,}$ and E are the Poisson's ratio, fracture toughness, and elastic modulus of the workpiece material,

respectively; C_2 is the dimensionless constant(C_2=0.226 [29]).

As seen in Fig.9, the fracture zone volume (V_0) of a single diamond grain corresponds to the $A_0A_1A_2A_3A_4$ pyramid. The effective scratching distance of a single grain per one vibration cycle during LTC-RUM (L) can be assessed as follows:

$$L = A_{\mathrm{T}} \sin(2\pi f t_c) + \frac{2\pi nR}{60} t_c \tag{13}$$

When a single grain length scratches on the workpiece surface, the grain penetration depth increases from zero to δ and then drops to zero. Consequently, the width and length of the lateral crack will increase from zero to the maximum value and then drops to zero. As a result, the theoretical material removal volume V_0 of the fracture zone can be calculated as:

$$V_0 = V_{A_0A_1A_2A_3A_4} = \frac{1}{3} C_L C_h L \tag{14}$$

During the LTC-RUM process, lateral cracks randomly propagate and interact as the grain impacts on the workpiece surface, increasing the differences between the actual (V) and the theoretical (V_0) values of the material removal volume per vibration cycle. To simplify the actual volume calculation, its value V is derived by multiplying V_0 to a constant adjusting coefficient K_{V}. Therefore, the material removal rate *MRR* of all grains in per vibration cycle can be expressed as:

$$MRR = K_V V_0 f N_a \tag{15}$$

In addition, the *MRR* can be obtained by the following equation.

$$MRR = \frac{\pi\left(d_o^2 - d_i^2\right)}{4} f_r \tag{16}$$

By equating Eqs. (14) and (15), and substituting Eqs. (6), (10), (12) and (13) into Eq. (14), it can be obtained :

$$F_c = \left[\frac{3 f_r H_V^{3/2} K_{\mathrm{IC}}^{1/2} (1-\upsilon^2)^{1/4} \lambda^{9/8} C_1^{1/8} C_a^{1/12} (d_o^2 - d_i^2)^{9/8} \left(\frac{\pi}{2} - \arcsin(1 - \frac{\delta}{A_L}) \right)^{9/8}}{4^{9/8} K_V f^{17/8} C_2^2 E^{7/8} S_a^{1/4} (\cot\psi)^{3/4} \left(A_T \sin(2\lambda(\frac{\pi}{2} - \arcsin(1 - \frac{\delta}{A_L}) + \frac{\lambda Rn}{30f}\left(\frac{\pi}{2} - \arcsin(1 - \frac{\delta}{A_L}) \right)\right)\right)} \right]^{8/9} \tag{17}$$

According to Eq. (17), the cutting force F_{c} can be determined by such processing parameters as spindle speed, feed rate, ultrasonic frequency and ultrasonic amplitude, tool parameters, and material properties in the LTC-RUM of brittle materials. In Eq.(17), F_{c} and δ are two unknown parameters if the adjusting coefficient K_{V} is determined by experiment. The relation between F_{c} and δ has been obtained by Eq.(11), and combining Eq.(17), the cutting force F_{c} and penetration depth δ can be acquired simultaneously.

4. Obtaining the adjusting coefficient K_{v}

4.1. Experimental setup

The rotary ultrasonic drilling tests were performed in this study using a modified CNC machine center (VMC850E) equipped with self-designed ultrasonic vibration devices. As presented in Fig.10, the experimental setup mainly comprised an ultrasonic vibration system, a cutting force measurement system, and a coolant system.

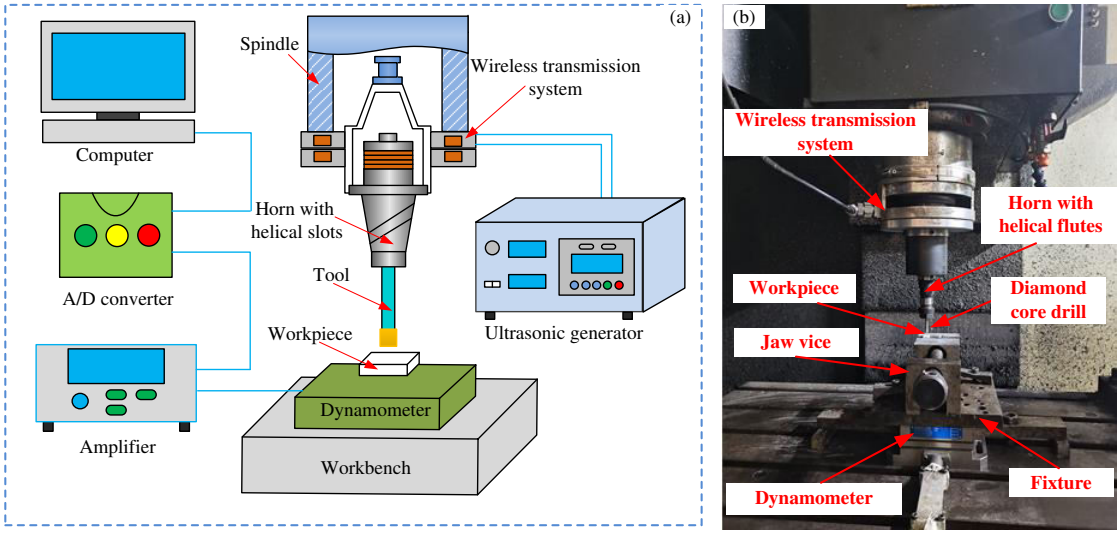

Fig.10. Experimental setup: (a) schematic diagram (b) primary setup

The ultrasonic vibration system included an ultrasonic generator, transducer, horn and an electroplated diamond core tool. The ultrasonic generator with a maximum output power of 500W converted the alternating current into high-frequency electric oscillation for the ultrasonic vibration system. Then, the piezoelectric transducer converted the electric oscillation into high-frequency mechanical vibration. However, the amplitude of mechanical vibration generated by the transducer was generally too low to be used for mechanical machining. Thus, the horn with helical slots used as concentrators amplified the ultrasonic vibration amplitude to applicable magnitudes. During the LTC-RUM, the longitudinal-torsional coupled vibration is applied to the end of the core drill, which is achieved by prefabricating four helical slots on the horn, as shown in Fig.11.

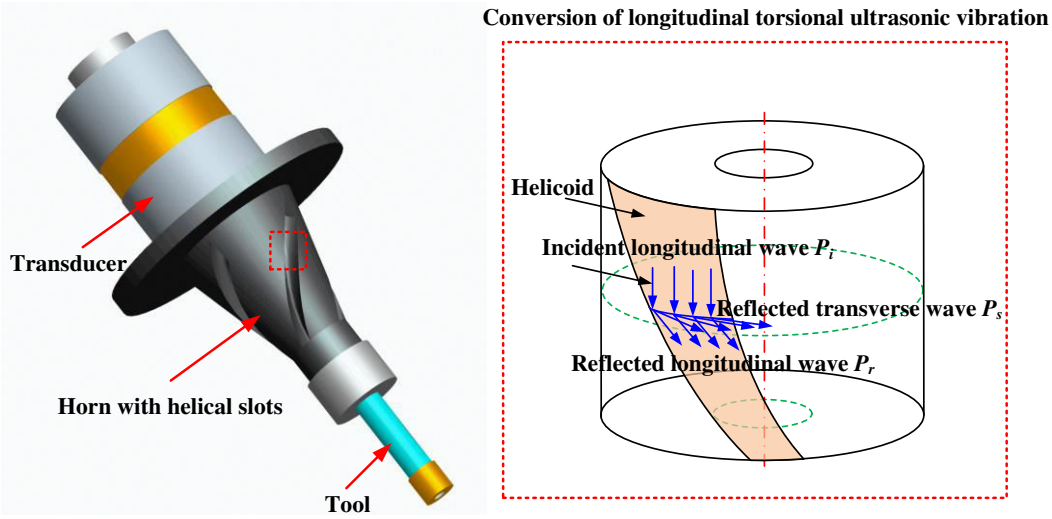

Fig.11. Illustration of longitudinal vibration conversion into torsional vibration.

When the ultrasonic wave generated by the transducer was transferred from the horn's larger end to the smaller ones, the reflection of waves occurred in the helical slots. As shown in Fig.11, under the action of helical slots, the incident longitudinal wave P_i was decomposed into the reflected longitudinal P_r and transverse P_s waves, respectively. Thus, the axial and circular components were produced at the horn's smaller end, including longitudinal and torsional vibrations, respectively. The mechanism of longitudinal vibration conversion into torsional one via helical slots was described in more detail in our earlier study [43], which findings were used to fabricate the horn with helical slots in this study. A laser displacement sensor (LK-G10, KEYENCE, Japan) was used to measure the torsional (A_T) and longitudinal (A_L) vibration amplitudes of the output end face, which ratio (A_T/A_L) is up to 0.52.

The diamond core tool was connected to the horn with an ER16 cone fit. The workpiece was fixed by a jaw vise grip and connected to a Kistler 9257B dynamometer through a fixture. As the forces in the x- and y- axis directions are smaller and substantially stable, the dynamometer was mounted on the worktable to measure the cutting force evolution along the z-axis direction during the test. A 4/8-channel laboratory charge amplifier (5070A) was used to amplify the electrical signal from the dynamometer, and then it was fed to a data recorder (2825A). Using the Dyno Ware data acquisition software produced by Kistler for cutting force measurement, the recorded data were stored and displayed via a PC. Because the dynamometer's natural frequency is much lower than the ultrasonic frequency, the average grinding force components were used to assess the processing.

4.2 Design of experiments

The workpiece material was zirconia ceramics, which mechanical properties are listed in Table 1. All workpiece-simulating specimens were machined to the initial dimensions of 15×10×5 mm.

Table 1. Mechanical properties of the zirconia ceramics material.

Properties	Unit	Value
Elastic modulus E	GPa	210
2Hardness H_V	GPa	12
Fracture toughness K_{IC}	MPa $m^{1/2}$	6
Density ρ	g/cm^3	6.05
Poisson's ratio υ		0.3

In the experiment, two tools named tools 1 and 2 were utilized to obtain the adjusting coefficient K_v and verify the cutting force model, respectively. The core tool parameters are listed in Table 2. The diamond core tool used in the experiment was manufactured by the Zhengzhou Research Institute for Abrasives & Grinding Co. Ltd, China. During the experiment, the workpiece mass before and after machining (including the machined cylinder) was weighted by a precision balance (JCS-2000).

Table 2. Core tool parameters.

Tool	Mesh size	Abrasive grain size S_a	Abrasive concentration C_a	Outer diameter d_o	Inner diameter d_i
Tool 1	#60-80	0.201	100	6.16	4.02
Tool 2	#80-100	0.162	100	8.19	6.24

During the experiment, when the tool's tuning length is 30 mm, the resonant frequency of tools 1 and 2 was 35.16 kHz and 35.12 kHz, respectively. The difference between the both tools can be neglected in the experiment. Due to the experimental set-up limitations, the ultrasonic vibration frequency was fixed for the both tools in the tests, while the spindle speed, feed rate, and ultrasonic amplitude were changed. The variation of ultrasonic amplitude for the tools 1 and 2 was achieved by adjusting the ultrasonic generator power. As depicted in Fig.12, the ultrasonic amplitude versus ultrasonic power curve was nearly linear.

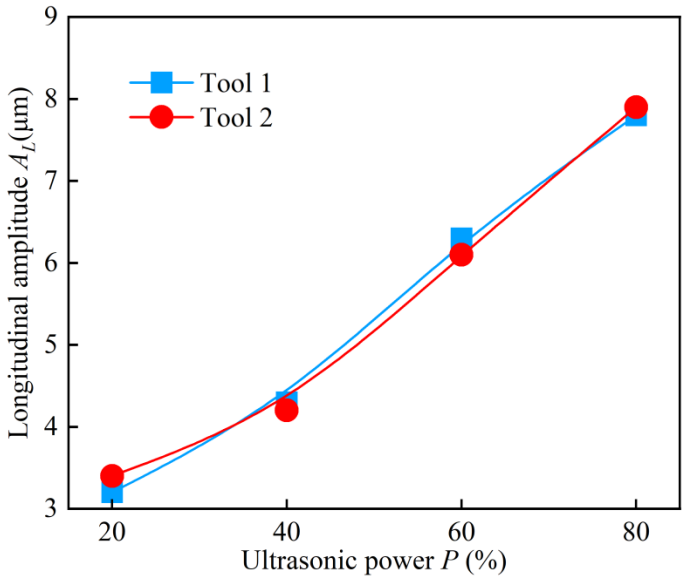

Fig.12. Experimental relationship between ultrasonic power and amplitude.

In order to obtain adjusting coefficient K_v, the detailed machining parameters are presented in Table 3. Each test was repeated three times, and a final value was obtained by averaging the measured results.

Table 3. Machining parameters.

Input variable	Unit	Values
Spindle speed (n)	r/min	2000,3000, 4000, 5000
Feed rate (f_r)	mm/min	5, 10, 15, 20
Ultrasonic power	%	20, 40, 60, 80

4.3 Analysis of experimental results

The actual volume (V) can be calculated using the following formula:

$$V = \frac{m_1 - m_2}{\rho f N_a} \tag{18}$$

where m_1 and m_2 is the workpiece mass values before and after machining (including the machined cylinder), respectively.

According to Liu et al. [12], the value of K_v varied only with the workpiece material, being independent of processing parameters. In this study, it was assessed via the following equation:

$$K_V = \frac{V}{V_0} = \frac{12H_V^{3/2}K_{IC}^{1/2}S_a{}^2(1-\upsilon^2)^{1/4}(m_1-m_2)}{\rho\pi f C_1 C_a{}^{3/2} C_2^2 (\cot\psi)^{3/4} E^{7/8} F_i^{9/8}(d_o^2-d_i^2)[A_T \sin(2\lambda(\frac{\pi}{2}-\arcsin(1-\frac{\delta}{A_L})+\frac{\lambda Rn}{30f}[\frac{\pi}{2}-\arcsin(1-\frac{\delta}{A_L})])} \quad (19)$$

Values of F_i in Eq.(18) could be derived via Eq.(4). According to Eq.(19), the relationship between the actual volume (V) and the theoretical volume (V_0) of material removal was obtained and plotted in Fig.13. The slope of the regression line, namely 0.239, can be utilized to assess K_V value.

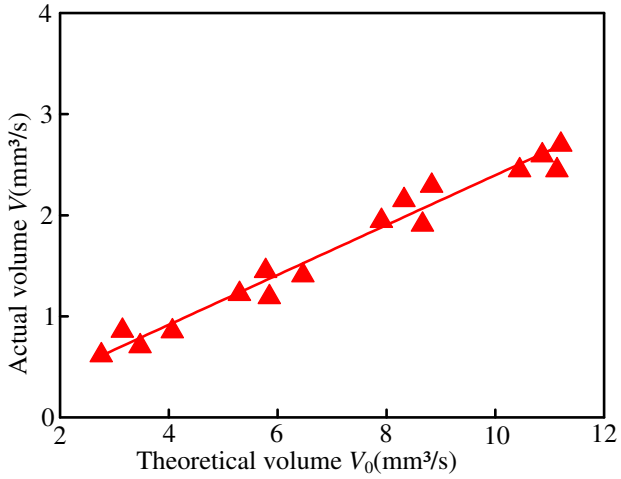

Fig.13. Correlation between the actual and theoretical material removal volumes V and V_0.

5. Cutting force prediction

Based on the developed mechanistic cutting force model，the cutting force can be predicted under the processing condition. Figure 14 present the predicted cutting forces with different machining variables. It can be seen that the predicted cutting force decreased with spindle speed and ultrasonic amplitude, but increased with the feed rate. According to Eq.(17), the cutting force F_c can be reduced by increasing spindle speed and ultrasonic amplitude (A_L and A_T), or decreasing the feed rate. In addition, according to Eq.(16), the *MRR* remains unchanged unless the feed rate is changed. In other words, the indentation depth δ needs to be decreased to keep the *MRR* unchanged with the spindle speed increasing. Besides, as shown in Fig.6 (a), a sparser cycloidal trajectory of a single abrasive grain implies that the indentation depth δ is reduced with the increase of spindle speed. Based on the Eqs.(3), (4), and (10), the indentation depth reduction leads to lower values of the effective contact time t_c and

the maximum impact force F_i, which effect further reduces the cutting force F_c. Therefore, with an increase in the spindle speed, the cutting force will decrease. Although the cycloidal trajectory of single abrasive grain slightly changes with the increase of feed rate, the workpiece's *MRR* will be promoted, increasing the corresponding indentation depth δ. In contrast to the spindle speed effect, an increase in the feed rate increases the cutting force F_c. The increasing of longitudinal amplitude will lead to larger indentation depth δ and maximum impact force F_i, but a smaller δ/A_L ratio [44]. This, in turn, will significantly reduce the effective contact time t_c, compensating the effect of increased maximum impact force F_i and resulting in the cutting force F_c eventual reduction. Moreover, as shown in Fig.8, under the action of the LTC vibration, the torsional ultrasonic amplitude A_T will cause the diamond abrasive particles to be vertically pulled out from the workpiece, improving their intermittent cutting effect. Therefore, larger longitudinal and torsional amplitude (A_L and A_T) are beneficial for cutting force reduction.

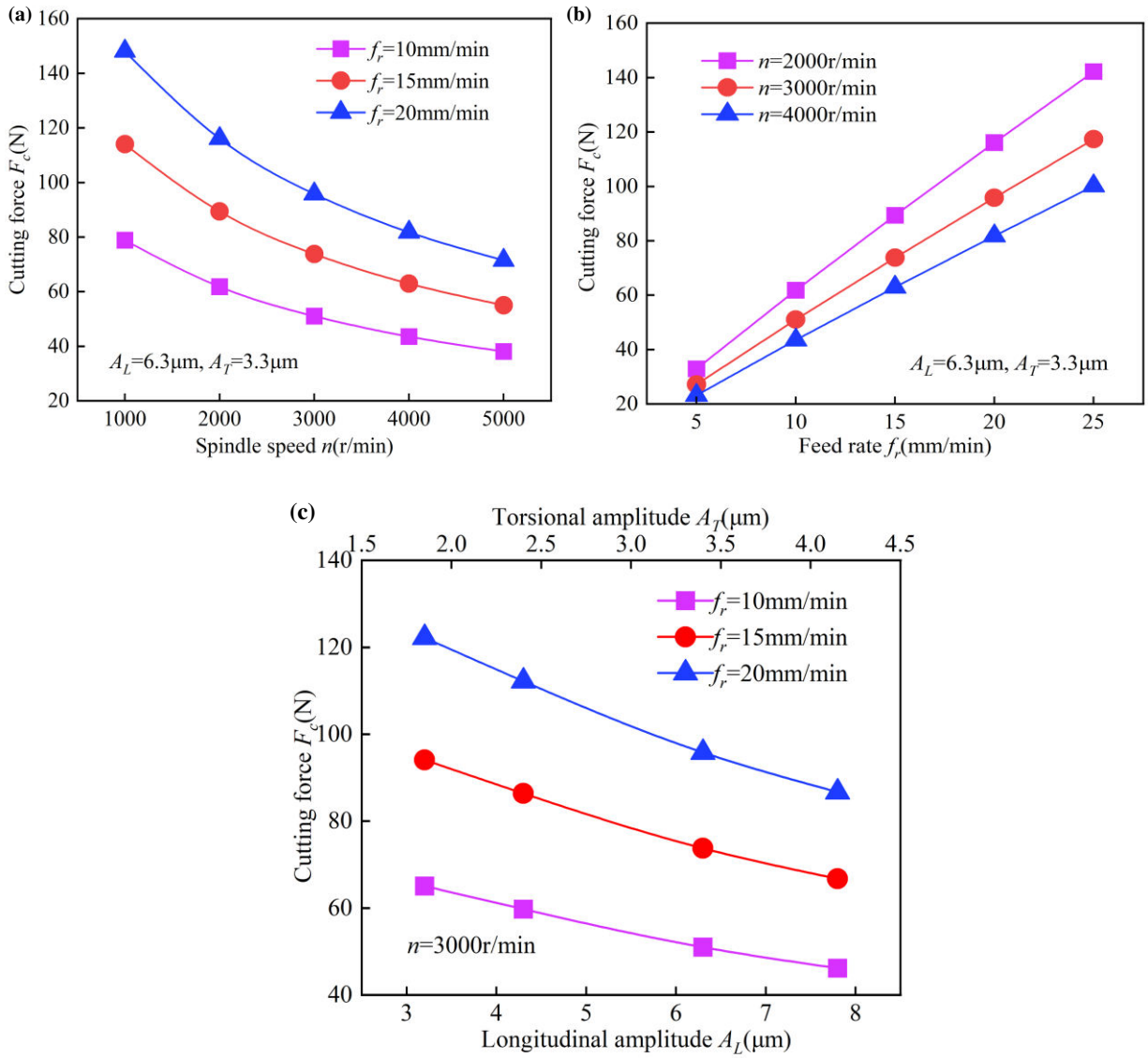

Fig.14. Prediction relation between parameters and cutting force (a) Spindle speed (b) Feed rate (c) Longitudinal and torsional amplitude

6. Pilot experimental verification

The pilot experiment was used to verify the cutting force modeling. The experimental setup was described in Section 4, and tool 2 was used in the test. The test parameters were shown in Table.4.

Table 4. Test parameters.

Input variable	Unit	Values
Spindle speed (n)	r/min	1000,2000,3000, 4000, 5000
Feed rate (f_r)	mm/min	5,10, 15, 20,25
Ultrasonic power	%	20, 40, 60, 80

Based on the developed mechanistic cutting force model，the cutting force can be predicted under the processing condition. Figure 15 compares the predicted and experimental cutting forces with different machining variables.

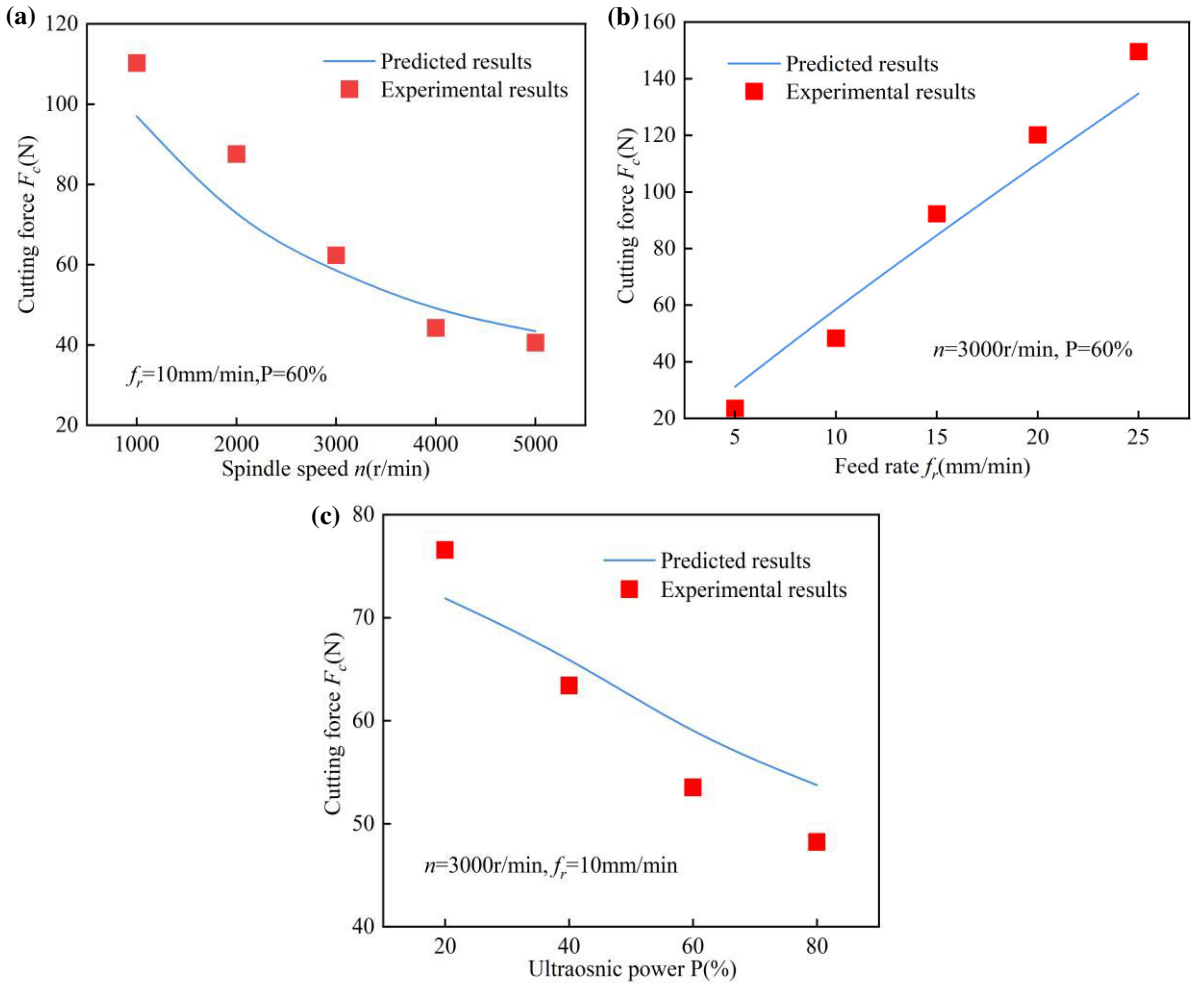

Fig. 15. Comparisons of the predicted and experimental cutting force versus various processing parameters: (a) spindle speed (b) feed rate (c) ultrasonic power

It can be seen that the predicted cutting force trends are closely correlated with the experimental ones. The cutting force decreased with spindle speed and ultrasonic power, but increased with the feed rate. Besides, the effect of spindle speed and feed rate on the cutting force is more obvious than ultrasonic power. The reasons were as follows: as shown in Fig 6, the abrasive grain trajectory is enhanced with the increase of spindle, which led to

reduce the penetration depth and further decrease the cutting force. The increased feed rate would increase the penetration depth, resulting in the cutting force increase. When the ultrasonic power is enhanced, the longitudinal and torsional amplitude is subsequently increased, and the intermittent cutting effect can be strengthened, which lead to the cutting force decrease. Compared with the less significant effect of ultrasonic amplitude on the cutting force in Con-RUM[12], its effect during the LTC-RUM is relative obvious. In addition, in order to obtain the optimal processing effect, it is essential to comprehensively select the processing parameter. It will be investigated in the future study.

7. Conclusions

In this study, an analytical cutting force model was proposed for the LTC-RUM processing of zirconia ceramics. The presented model's feasibility was validated by the actual LTC-RUM tests. The following conclusions can be drawn:

(1) The kinematic motion of a single abrasive grain and its interaction with the processed workpiece were analyzed. It was found that LTC vibration could improve the intermittent cutting effect of a single abrasive grain, and the material removal mechanism can be changed.

(2) In this study, the LTC-RUM technique was successfully implemented by prefabricating helical slots in the horn. Based on the wave conversion mechanism, the incident longitudinal wave was decomposed to reflect longitudinal and transverse waves, respectively, providing the required LTC vibration at the output end of the core tool.

(3) The cutting force variation under various processing parameters was analyzed based on the material removal mechanism of brittle fracture, and experimentally validated. The cutting force exhibited a negative correlation with spindle speed and ultrasonic power (amplitude), as well as a positive correlation with feed rate.

Declarations

Authors' contribution Fan Chen and Wenbo Bie conceived the analysis and wrote the manuscript. Bo Zhao provided supervisions on experimentation and manuscript preparation. Yingli Chang and Xiaobo Wang collected the data and revised the manuscript. Wenbo Bie, Yingli Chang and Yuemin Zhang performed the experiment. The authors discussed each reference paper together and contributed useful ideas for this manuscript.

Funding This work was financially supported by the National Natural Science Foundation of China (Nos. 51805284, 52005164), the Key R&D and Promotion Program (Science and Technology) in Henan Province, China (No. 20202102210266),and PhD Research Start-up Fund Project of Pingdingshan University of China (No.PXY-BSQD-2022001).

Availability of data and material All data generated or analyzed during this study are included in the present

article.

Ethical approval The article follows the guidelines of the Committee on Publication Ethics (COPE) and involves no studies on human or animal subjects.

Consent to participate Not applicable.

Consent to publish Not applicable.

Competing interests The authors declare that no potential conflicts of interest with respect to the research, authorship, and/or publication of this article.

References

[1] Zahedi A, Tawakoli T, Akbari J (2015) Energy aspects and workpiece surface characteristics in ultrasonic-assisted cylindrical grinding of alumina-zirconia ceramics. Int J Mach Tools Manuf 90: 16-28.

[2] Xiao XZ, Zheng K, Liao WH, Meng H (2016) Study on cutting force model in ultrasonic vibration assisted side grinding of zirconia ceramics. Int J Mach Tools Manuf 104: 58-67.

[3] Wdowik R, Porzycki J, Magdziak M (2017) Measurements of surface texture parameters after ultrasonic assisted and conventional grinding of ZrO2 based ceramic material characterized by different states of sintering. Procedia CIRP 62: 293-298.

[4] Yang ZC, Zhu LD, Lin B, Zhang GX, Ni CB, Sui TY (2019) The grinding force modeling and experimental study of ZrO 2 ceramic materials in ultrasonic vibration assisted grinding. Ceram Int 45: 8876-8839.

[5] Yang M, Li CH, Zhang YB, Jia DZ, Li RZ, Hou YL, Cao HJ (2019) Effect of friction coefficient on chip thickness models in ductile-regime grinding of zirconia ceramics. Int J Adv Manuf Technol 102: 2617-2632.

[6] Yang M, Li CH, Zhang Y, Zhang XP, Li RZ, Hou YL, Wang J (2017) Maximum undeformed equivalent chip thickness for ductile-brittle transition of zirconia ceramics under different lubrication conditions. Int J Mach Tools Manuf 122:55-65.

[7] Xu S, Yao ZQ, Cai HY, Wang HY (2017) An experimental investigation of grinding force and energy in laser thermal shock-assisted grinding of zirconia ceramics, Int. J. Adv. Manuf. Technol. 91:3299-3306.

[8] Suzuki T, Ohmori H, Dai Y, Lin W.M, Katahira K, Makinouchi A, Tashiro H, Yokota H, Suzuki M, Abe T, Shimasaki T (2003) Ultraprecision fabrication of glass ceramic aspherical mirrors by ELID-grinding with a nano-level positioning hydrostatic drive system. Key Eng Mater 238: 49-52.

[9] Agarwal S (2015) On the mechanism and mechanics of material removal in ultrasonic machining. Int J Mach Tools Manuf 96:1-14.

[10] Yang ZC, Zhu LD, Zhang GX, Ni CB, Lin B (2020) Review of ultrasonic vibration-assisted machining in advanced materials. Int J Mach Tools Manuf 156: 103594.

[11] Singh RP, Singhal S (2016) Rotary Ultrasonic Machining: A Review. Mater Manuf Processes 31: 1795-1824.

[12] Liu DF, Cong WL, Pei ZJ (2012) A cutting force model for rotary ultrasonic machining of brittle materials. Int J Mach Tools Manuf 52 (1): 77-84.

[13] Wang JJ, Feng PF, Zhang JF, Zhang CL, Pei ZJ (2016) Modeling the dependency of edge chipping size on the material properties and cutting force for rotary ultrasonic drilling of brittle materials. Int J Mach Tools Manuf 101: 18-27.

[14] Cao JG, Wu YB, Lu D, Fujimoto M, Nomura M (2014) Material removal behavior in ultrasonic-assisted scratching of SiC ceramics with a single diamond tool. Int J Mach Tools Manuf 79: 49-61.

[15] Zhang CL, Feng PF, Zhang JF (2013) Ultrasonic vibration-assisted scratch-induced characteristics of C-plane sapphire with a spherical indenter. Int J Mach Tools Manuf 64: 38-48.

[16] Singh RP, Singhal S (2017) Rotary ultrasonic machining of macor ceramic: An experimental investigation and microstructure analysis. Mater Manuf Processes 32: 927-939.
[17] Lv DX, Wang HX, Tang YJ, Huang YH, Zhang HJ, Ren W (2012) Surface observations and material removal mechanisms in rotary ultrasonic machining of brittle material. Proc Inst Mech Eng, Part B: J Eng Manuf 226 (9): 1479-1488.
[18] Jain AK, Pandey PM (2016) Study of peck drilling of borosilicate glass with μ-RUM process for MEMS. J Manuf Processes. 22: 134-150.
[19] Nath C, Lim GC, Zheng HY (2012) Influence of the material removal mechanisms on hole integrity in ultrasonic machining of structural ceramics. Ultrasonics. 52 (5): 605-613.
[20] Ding K, Fu YC, Su HH, Chen Y, Yu XZ, Ding GZ (2014) Experimental studies on drilling tool load and machining quality of C/SiC composites in rotary ultrasonic machining. J Mater Process Technol (12): 2900-2907.
[21] Wang H, Hu YB, Cong WL, Hu ZL (2019) A mechanistic model on feeding-directional cutting force in surface grinding of CFRP composites using rotary ultrasonic machining with horizontal ultrasonic vibration. Int J Mech Sci 155: 450-460.
[22] Zhang CL, Zhang JF, Feng PF (2013) Mathematical model for cutting force in rotary ultrasonic face milling of brittle materials. Int J Adv Manuf Technol 69(1-4): 161-170.
[23] Ning FD, Wang H, Cong WL, Fernando PKSC (2017) A mechanistic ultrasonic vibration amplitude model during rotary ultrasonic machining of CFRP composites. Ultrasonics. 76: 44-51.
[24] Bertsche E, Ehmann K, Malukhin K (2013) An analytical model of rotary ultrasonic milling. Int J Adv Manuf Technol 65 (9-12): 1705-1720.
[25] Wang JJ, Zhang CL, Feng PF, Zhang JF (2016) A model for prediction of subsurface damage in rotary ultrasonic face milling of optical K9 glass. Int J Adv Manuf Technol 3(1-4): 347-355.
[26] Wang JJ, Zha HT, Feng PF, Zhang JF (2016) On the mechanism of edge chipping reduction in rotary ultrasonic drilling: A novel experimental method. Precis Eng 44: 231-235.
[27] Geng DX, Liu YH, Shao ZY, Zhang ML, Jiang XG, Zhang DY(2019) Delamination formation and suppression during rotary ultrasonic elliptical machining of CFRP. Composites Part B 183: 107698.
[28] Wang JJ, Zhang JF, Feng PF, Guo P (2018) Damage formation and suppression in rotary ultrasonic machining of hard and brittle materials: a critical review. Ceram Int 44(2): 1227-1239.
[29] Wang JJ, Zhang JF, Feng PF, Guo P (2018) Experimental and theoretical investigation on critical cutting force in rotary ultrasonic drilling of brittle materials and composites. Int J Mech Sci 135: 555-564.
[30] Fernando PKSC, Zhang M, Pei ZJ (2019) Rotary ultrasonic machining: effects of tool natural frequency on ultrasonic vibration amplitude. Mach Sci Technol 23(4): 595-611.
[31] Cong WL, Feng Q, Pei ZJ, Deines TW, Treadwell C (2012) Rotary ultrasonic machining of carbon fiber-reinforced plastic composites: using cutting fluid vs. cold air as coolant. J Compos Mater 46(14): 1745-1753.
[32] Churi N. (2010) Rotary ultrasonic machining of hard-to-machine materials. Manhattan: Kansas State University.
[33] Cong WL, Pei ZJ, Deines TW, Srivastava A, Riley L, Treadwell C (2012) Rotary ultrasonic machining of CFRP composites: A study on power consumption. Ultrasonics. 52(8) : 1030-1037.
[34] Tang XT, Liu YX, Shi SJ, Chen WS (2017) Development of a novel ultrasonic drill using longitudinal-bending hybrid mode. IEEE Access 5: 7362-7370.
[35] Geng DX, Lu ZH, Yao G, Liu JJ, Li Z, Zhang DY (2017) Cutting temperature and resulting influence on machining performance in rotary ultrasonic elliptical machining of thick CFRP. Int J Mach Tools Manuf 123: 160-170.

[36] Xu W, Zhang L (2015) Ultrasonic vibration-assisted machining: principle, design and application. Adv Manuf 3(3): 173-192.

[37] Gao GF, Xia ZW, Yuan ZJ, Xiang DH, Zhao B (2021) Influence of longitudinal-torsional ultrasonic-assisted vibration on micro-hole drilling Ti-6Al-4V. Chin J Aeronaut 34 (9): 247-260.

[38] Liu J, Chen G, Ren CZ, Qin XD, Zou YH, Ge JY (2020) Effects of axial and longitudinal-torsional vibration on fiber removal in ultrasonic vibration helical milling of CFRP composites. J Manuf Processes 58: 868-883.

[39] Andrea C, Patrick H, Margaret L (2010) Ultrasonic rock sampling using longitudinal-torsional vibrations, Ultrasonics. 50(4-5) : 447-452.

[40] Wang JJ, Zhang JF, Feng PF, Guo P (2018) Reducing cutting force in rotary ultrasonic drilling of ceramic matrix composites with longitudinal-torsional coupled vibration. Manuf Lett 18: 1-5.

[41] Ma WJ, Xue JX, Yang YH, Zhao H, Hu GH, Long ZL (2020) Kinematics characteristics and experimental analysis of longitudinal torsional ultrasonic grinding for Zirconia ceramics. Mech Sci Technol Aerosp Eng 39(10): 1580-1586.

[42] Wang JJ, Zhang JF, Feng PF, Guo P, Zhang QL (2018) Feasibility study of longitudinal-torsional-coupled rotary ultrasonic machining of brittle material. ASME J Manuf Sci Eng 140(5): 051008.

[43] Zhao B, Bie WB, Wang X, Chen F, Chang BQ (2019) Design and experimental investigation on longitudinal-torsional composite horn considering the incident angle of ultrasonic wave. Int J Adv Manuf Technol 105(1-4): 325-341.

[44] Cong WL, Pei ZJ, Sun X, Zhang CL (2014) Rotary ultrasonic machining of CFRP: A mechanistic predictive model for cutting force. Ultrasonics 54(2): 663-675.